

# Investigating Ca II emission in the RS CVn binary ER Vulpeculae using the Broadening Function Formalism

Evgenya Shkolnik

*NASA Astrobiology Institute, University of Hawaii at Manoa, 2565 McCarthy Mall, Rm.  
213, Honolulu, HI 96822, U.S.A.*

shkolnik@hawaii.edu

Gordon A.H. Walker<sup>1</sup>

*1234 Hewlett Place, Victoria, BC, Canada, V8S 4P7*

gordonwa@uvic.ca

Slavek M. Rucinski<sup>1</sup>

*David Dunlap Observatory, University of Toronto, P.O.Box 360, Richmond Hill, ON,  
Canada L4C 4Y6*

rucinski@astro.utoronto.ca

David A. Bohlender and Tim J. Davidge

*National Research Council of Canada, Herzberg Institute of Astrophysics  
5071 West Saanich Road Victoria, BC, Canada V9E 2E7*

david.bohlender@nrc.ca, tim.davidge@nrc.ca

## ABSTRACT

The synchronously rotating G stars in the detached, short-period (0.7 d), partially eclipsing binary, ER Vul, are the most chromospherically active solar-type stars known. We have monitored activity in the Ca II H & K reversals for almost an entire orbit. Rucinski's Broadening Function Formalism allows the photospheric contribution to be objectively subtracted from the highly blended spectra. The power of the BF technique is also demonstrated by the good agreement of radial velocities with those measured by others from less crowded spectral

---

<sup>1</sup>Visiting Astronomer, Canada-France-Hawaii Telescope, operated by the National Research Council of Canada, the Centre National de la Recherche Scientifique of France, and the University of Hawaii.

regions. In addition to strong Ca II emission from the primary and secondary, there appears to be a high-velocity stream flowing onto the secondary where it stimulates a large active region on the surface  $30 - 40^\circ$  in advance of the sub-binary longitude. A model light curve with a spot centered on the same longitude also gives the best fit to the observed light curve. A flare with  $\sim 13\%$  more power than at other phases was detected in one spectrum. We suggest ER Vul may offer a magnified view of the more subtle chromospheric effects synchronized to planetary revolution seen in certain ‘51 Peg’-type systems.

*Subject headings:* stars: activity, binaries: eclipsing, binaries: spectroscopic, stars: individual: ER Vul

## 1. Introduction

RS Canum Venaticorum systems (RS CVn) are (normally) contact binaries with two active late-type stars having orbital periods between 2 and 20 days (Hall 1992). Both components have strong chromospheric, transition region and coronal emission. This is generally assumed to be the result of a powerful dynamo action caused by rapid rotation and deep convection zones leading to magnetic activity several orders of magnitude greater than the Sun’s (Vogt et al. 1999).

ER Vulpeculae is a bright, well-studied RS CVn system which we chose to test our observation that certain ‘51 Peg’-type planets induce detectable chromospheric activity on their parent stars through magnetic interaction (Shkolnik et al. 2003, 2004). We observed Ca II H (3967 Å) and K (3933 Å) emission as the primary optical indicators of chromospheric activity because the stellar Ca II H and K photospheric absorption lines are so broad and deep that the reversals are seen in high contrast against the shallow stellar core ( $\sim 10\%$  of the continuum). ER Vul’s short orbital period, brightness ( $V = 7.4$ ), and high level of chromospheric emission makes it an ideal target for observing phase-dependent variability.

This tidally-synchronized binary is unusual in that it consists of two solar-type stars orbiting each other with a relatively short period of 0.698 days. The stars are nearly identical (G1-2 V and G3 V) with equal radii ( $1.07 R_\odot$ ) and a mass ratio of 0.947. They are only  $3.97 R_\odot$  apart in a circular orbit but they are not in contact. The orbital inclination of  $67^\circ$ , this configuration leads to partial eclipses of approximately 12% (Gunn & Doyle 1997). The projected rotational velocities of the primary and secondary components are  $(v \sin i)_P = 97.4 \pm 1.3 \text{ km s}^{-1}$  and  $(v \sin i)_S = 96.7 \pm 2.2 \text{ km s}^{-1}$  (Duemmler et al. 2003). This rapid rotation causes very broad and blended features in the double-lined spectrum.

ER Vul has been studied in almost every spectral region to discover, map and understand its intense stellar and circumstellar activity. Piskunov (1996) used Doppler imaging to map the surfaces of both stars from 12 high-resolution spectra centered on 6440 Å at the Nordic telescope. He identified hot spots on both components at sub-stellar longitudes, which he presumed to be due to reflection.

Duemmler et al. (2003) also report phase-dependent activity on ER Vul from asymmetry in the Ca II IRT line at 8662 Å. They measured deviations of  $\sim 10$  km s<sup>-1</sup> from the radial velocity (RV) curve at phases when a star is receding from the observer. They suggest that this is caused by localized excess emission near the sub-binary point on the star. Alternatively, a weakening of the emission at opposite orbital phases could produce the same effect. They measured a higher level of activity on the cooler, secondary component, which was already known to be globally more active than the primary (Gunn & Doyle 1997; Çakirli et al. 2003).

VLA radio observations by Rucinski (1992, 1998) revealed a complex, relatively large radio flux variability but having no clear correlation with the orbital period. This may indicate a structured radio corona. At the other extreme, EXOSAT observations exhibit a homogeneous X-ray corona (White et al. 1987). The lack of any eclipses in these two wavelengths can be interpreted as either the active regions are at high latitudes or the regions of X-ray and radio emission extend quite far beyond the binary system, perhaps in the form of huge coronal loops.

The classic chromospheric diagnostics, Ca II H & K, were looked at by Montes et al. (1996) and Fernandez-Figueroa et al. (1994) as part of a large survey of chromospherically active binaries. However, their data were too few and sporadic to make any claims of phase-dependent activity. In this paper, we present 42 new Ca II H & K observations with nearly complete orbital phase coverage. The details of the observations are discussed Section 2. In Section 3, we present the broadening functions (BFs) determined from the spectra with the derived RVs and the orbital parameters. The Ca II emission is isolated using the BFs and its origins are discussed in Section 4. In Section 5, we model the photometric lightcurve obtained concurrently with the spectroscopic observations.

## 2. The ER Vul Spectra

Ca II H & K spectra were taken at the Canada-France-Hawaii Telescope (CFHT) with the Gecko échellette spectrograph fiber fed by CAFE (CAssegrain Fiber Environment) from the Cassegrain to Coudé focus (Baudrand & Vitry 2000). Spectra were centered at 3947

Å which was isolated by a UV grism (300 lines  $\text{mm}^{-1}$ ) with  $\simeq 60$  Å intercepted by the CCD. The dispersion was  $0.0136 \text{ Å pixel}^{-1}$  and the 2.64-pixel FWHM of the thorium-argon (Th/Ar) lines corresponded to a spectral resolution of  $R = 110,000$ . The detector was a back-illuminated EEV CCD ( $13.5 \mu\text{m}^2$  pixels,  $200 \times 4500$  pixels) with spectral dispersion along the rows of the device. The B magnitude of ER Vul is 7.93 allowing a S/N of  $\sim 180 \text{ pixel}^{-1}$  (or  $1500 \text{ Å}^{-1}$ ) to be achieved in an exposure time of 1200 s. We used the same set-up for ER Vul as we did for the ‘51-Peg’ systems presented in Shkolnik et al. (2003) where the reduction details can be found in Section 3 of that paper.

Of the three nights awarded, two were clear (2002 August 26 and 27), giving us almost complete phase coverage,  $\phi = 0.09 - 0.96$ . Table 1 lists the heliocentric Julian date (HJD) and orbital phase of each exposure. Harmanec et al. (2004) supplied an updated ephemeris from photometric monitoring done at two observatories in Hvar, Croatia and Victoria, Canada. The time of primary eclipse ( $\phi = 0$ ), occurred at  $\text{HJD} = 2440182.25628(46)$ <sup>1</sup> with a period of  $0.698095113(29)$  d. Specimen ER Vul spectra are shown in Figure 1 at the three phases  $\phi = 0.25, 0.50$  and  $0.62$ .

### 3. The Broadening Functions

For a close binary with rapidly rotating components such as those of ER Vul, the Broadening Function (BF) approach is optimal to obtain radial velocity information for one-dimensional, radial-velocity domain images of the stellar surfaces. The broadening function approach was used for the first time in 1992 (Rucinski 1992) and subsequently, for analysis of radial velocities of close binary stars. The technical summaries are in Rucinski (1999) and Rucinski (2002). The BF method uses a spectrum of a chromospherically inactive star as a template. The template could either be a synthetic spectrum or a real spectrum of a sharp-lined (slowly rotating) star that is artificially Doppler broadened by the BFs. Subtracting a broadened template spectrum from that of an active binary leaves only emissions from stellar active regions such as plages or prominences.

The principal properties of the approach, described in detail in Rucinski (1992, 1999, 2002)<sup>2</sup>, are based on the fact that the observed spectrum of a rapidly-rotating or revolving star can be approximated by a convolution of a sharp-line star spectrum with a kernel describing the observed radial velocity field. Thus, the broadening function  $B$ , in  $P = S * B$ ,

---

<sup>1</sup>Values in brackets are  $1\sigma$  errors.

<sup>2</sup>See also <http://www.astro.utoronto.ca/~rucinski>.

is a kernel in  $P(\lambda') = \int B(\lambda' - \lambda) S(\lambda) d\lambda$ . In this integral equation,  $P$  is the “program” spectrum and  $S$  is the “sharp” or the template spectrum. The equation can be solved by representing the convolution operation by a set of over-determined algebraic equations;  $S$  &  $P$  are usually defined over thousands of pixels, while  $B$  is usually defined over hundreds of pixels, so the equations can be cast as a standard least-squares problem with an over-determinacy typically of  $> 10$  times.

The use of a radial velocity standard star of similar spectral type for the template  $S$  straightforwardly relates the results to the velocity scale and insures the use of all, even the weakest, lines which would not appear in model spectra; this property is similar to that of the Cross-Correlation Function (CCF). However, the resolution of the BF depends on and is entirely defined by the instrumental setup, which is a great advantage over the CCF which combines all sources of broadening. This frequently leads to the necessity of excising wide hydrogen lines, molecular features, etc. The BF is derived through a linear process, so that its features can be used directly for estimates of the the relative light intensities. A very similar technique, called the Least Squares Deconvolution (LSD), was developed mainly for magnetic Zeeman pattern extraction by Donati et al. (1997) and then used for radial velocity and line broadening applications (e.g. Collier Cameron et al. 2002, Reiners & Schmitt 2003). Both techniques use the Singular Value Decomposition for determination of the spectral line locations and broadening, but the LSD is typically used with model spectra while the BF formalism relies on stellar templates for direct tie-ins to the radial velocities of standard stars and accounts for weak lines not present in model spectra.

For a close binary like ER Vul, the BF is essentially a projection of the system into the radial velocity domain. If stars are spherical and rotate rigidly, the BF is expected to have the ellipsoidal shape predicted by the Struve profile (Solana & Frenley 1997). Spots will appear as notches in the BF at certain velocities. It is important to recognized that any emission components will appear as dark notches, which is perhaps somewhat less intuitive; however, we do not expect any emission components in the photospheric lines used to determine the BFs in this study.

We used the average spectrum of HD 209458, formed from three spectra taken a few weeks prior to our 2002 August observing run, as the template (standard) star with which to calculate the BFs for the ER Vul spectra. HD 209458 is a G0 V star making it a good match to both of ER Vul’s components. Computations of the BFs involve inversion of large matrices. The computing time can be reduced if the spectra are reduced in length by re-sampling to lower resolution. The full resolution of 0.013 Å per pixel (0.95 km s<sup>-1</sup>) was deemed unnecessary; we reduced it two-fold to the velocity step of 1.9 km s<sup>-1</sup>. Considering that the spectral features of ER Vul are very broad, there is no significant loss of information

from this step. The total number of useful pixels in the equal-velocity-step spectra was 2250 (at  $1.9 \text{ km s}^{-1}$ ), while the wide range of the ER Vul velocities dictated a relatively large spectral window of  $700 \text{ km s}^{-1}$  or 369 pixels. Thus, the overall over-determinacy in the BF solutions was moderate, 6 times, which was adequate to provide high-quality BF profiles.

Only the upper 2/3 of the ER Vul spectrum (as measured from the peak flux of the pseudo-continuum from in between the two strong Ca II lines) was used in the calculations of the BFs in order to exclude the Ca II reversals and to eliminate any departures from the photospheric component due to chromospheric activity. Besides, only the well defined upper parts of the spectra found in regions between and outside the Ca II cores, which are rich in narrow lines, could provide a good basis for the BF determination.

The most difficult and unusual step in the BF determination was the normalization of the strongly curved spectrum outside the Ca II features. The spectra of ER Vul are severely blended and there are no places where we can see the photospheric continuum. The normalization was done by an interactive determination of the upper envelope to the spectrum and division of the spectra by such an approximate continuum. That this is not the actual photospheric continuum is clearly indicated by the sums of the BFs which, in spite of the spectral type of the template (G0V) matching very well with the of the components of ER Vul, are not close to unity for each component, but are instead at the level of  $\simeq 0.35$ . This means that about 2/3 of the total amount of absorption in the spectral lines of ER Vul is located in unaccounted-for line blends. The combined effect of the blending is the lowering of the effective continuum and shallower depths of those lines that remain visible. Because this is still a linear transformation and the broadening functions are determined through a linear process, the total intensities of the BFs are affected while the shapes and positions of the BFs remain entirely unchanged. As a final step, we normalized the total intensities to 1.

The final BFs are very well defined and clearly show both of the components. All determined BFs are plotted in Figure 2. Figure 3 provides a closer look at the BFs at  $\phi = 0.25, 0.50$  and  $0.62$ . We can determine RVs and hence the system orbital parameters from the BFs as measured in the next section. We do not see any evidence of bright or dark spots on the stellar surfaces which would appear as travelling notches in the BFs implying that more than 50% of the stellar disk may be covered by one or more spots. This is consistent with Sokoloff & Piskunov (2002) who observe a large, high-latitude cool spots on ER Vul.

Table 1. ER Vul: 2002 August Observations

HJD - 2452000	Orbital Phase	RV (P) <sup>a</sup> km s <sup>-1</sup>	RV (S) <sup>a</sup> km s <sup>-1</sup>
512.773	0.090	-86.0	65.4
512.789	0.113	-99.3	82.9
512.806	0.137	-113.5	92.1
512.822	0.160	-124.5	101.5
512.839	0.184	-132.7	115.5
512.855	0.207	-138.3	121.7
512.871	0.230	-141.2	126.0
512.887	0.253	-143.6	125.4
512.903	0.276	-145.1	126.9
512.919	0.299	-137.1	119.9
512.935	0.321	-130.2	116.3
512.950	0.344	-121.7	106.6
512.967	0.367	-112.8	93.1
512.983	0.390	-102.1	82.5
512.999	0.414	-71.8	73.9
513.015	0.437	-21.3	60.6
513.031	0.460	-14.1	-14.1
513.047	0.482	-14.8	-14.6
513.063	0.505	-13.7	-13.7
513.734	0.467	-16.8	-16.4
513.750	0.489	-15.0	-15.4
513.766	0.512	-13.3	-14.4
513.782	0.535	-7.6	-8.1
513.798	0.558	0.4	0.7
513.814	0.581	39.7	-79.1
513.829	0.603	71.3	-100.3
513.845	0.626	81.9	-116.3
513.861	0.648	92.3	-128.3
513.877	0.671	103.3	-137.9
513.893	0.694	109.1	-146.3
513.909	0.717	117.1	-149.5
513.924	0.739	112.5	-148.5
513.940	0.761	114.2	-154.6
513.955	0.784	112.7	-147.4
513.971	0.806	104.9	-142.6
513.987	0.829	101.6	-134.2

Table 1—Continued

HJD – 2452000	Orbital Phase	RV (P) <sup>a</sup> km s <sup>-1</sup>	RV (S) <sup>a</sup> km s <sup>-1</sup>
514.003	0.852	88.3	-122.2
514.019	0.875	77.6	-108.4
514.035	0.898	68.4	-94.6
514.051	0.920	43.4	-68.1
514.066	0.942	1.9	2.0
514.082	0.965	-8.5	-8.8

<sup>a</sup>RV measured from the centroid of the BF.



### 3.1. Radial Velocities from the BFs

Even though RV curves for the ER Vul system have been measured repeatedly, we demonstrate the quality and extent of information one can extract from the BFs. Despite the severe line blending and the limited spectral range, we were able to determine good RV curves from the BFs. We measured radial velocities (RVs) for each component of ER Vul by fitting Gaussian curves to the BFs of each star at each phase. The velocity at the line centroid was measured with an uncertainty of  $0.5 \text{ km s}^{-1}$ . The RV curve as a function of phase is plotted in Figure 4. The RVs near conjunction ( $0.9 \leq \phi \leq 0.1$  and  $0.4 \leq \phi \leq 0.6$ ) are inaccurate because only one Gaussian could be fitted to the blended BFs. The solid curves are sine functions using the system parameters measured by Duemmler et al. (2003). The velocity amplitudes of the primary and secondary components are  $K_P = 135.20 \pm 0.63 \text{ km s}^{-1}$  and  $K_S = 142.82 \pm 0.76 \text{ km s}^{-1}$ , the eccentricity  $e = 0$  and the systemic velocity  $\gamma = 25.49 \pm 0.39 \text{ km s}^{-1}$ . The dashed curves are the best-fitting sine functions to the data using the RVs outside of the conjunction region. For these,  $K_P = 130.55 \text{ km s}^{-1}$ ,  $K_S = 140.25 \text{ km s}^{-1}$ ,  $e = 0$  and  $\gamma = 26.68 \text{ km s}^{-1}$ . The RMS scatter of the data relative to the solid curves are  $6.15 \text{ km s}^{-1}$  for the primary and  $4.30 \text{ km s}^{-1}$  for the secondary. The deviation of the primary by  $\approx -10 \text{ km s}^{-1}$  at  $\phi \approx 0.75$  may be due to spectral line distortions caused by less stellar activity relative to the rest of the star and could be an indication of relatively *inactive* longitudes. The RV of the secondary also deviates at its maximum, but only by  $\approx -5 \text{ km s}^{-1}$ .

## 4. Ca II Emission in the ER Vul System

### 4.1. Extracting the K Emission

The rapid rotation and orbital velocities of the two components of ER Vul introduce severe Doppler broadening and line blending making it difficult to distinguish the contribution from each star separately. The BF technique allows the chromospheric emission for each star to be isolated from the rest of the stellar flux by subtracting a template spectrum convolved with the appropriate BF. Figure 5 illustrates the steps involved at a given phase: (a) the sharp-lined spectrum of HD 209458 that we used as our standard, (b) the BF measured from the ER Vul spectrum at  $\phi = 0.25$  (quadrature), (c) the convolution of the BF with the sharp-lined template, and (d) the observed ER Vul spectrum at  $\phi = 0.25$ .

This procedure to remove the photospheric contribution to the spectrum works well as is seen in the residual spectrum (with no normalization) in Figure 6. The three origins of H & K emission remain: the chromospheres of the primary and secondary stars, and a broad

emission which, at this phase ( $\phi = 0.25$ ), is highly redshifted. Unfortunately, the 60-Å-wide spectrum cuts off the broad emission red-ward of the H line so we will not discuss the H emission much further as it suffers from truncation in the convolution. The fluctuations seen in the figure between the H and K lines (1800 – 3200 km s<sup>-1</sup>) are most likely due to two processing issues: 1) the spectral type of HD 209458 matches ER Vul’s primary star very well, but differs by 3 sub-classes for the secondary; and 2) when comparing broad-lined spectra with highly-blended features, the normalization becomes a tricky task. This challenge arises during the calculation of the BFs and then again when setting the pseudo-continuum level of the standard and stellar spectra before subtraction. The stellar and template spectra used to produce Figure 6, were merely set to the same maximum level. The larger fluctuations in this region may also be attributed to the presence of the large, high-latitude cool spots observed by Sokoloff & Piskunov (2002). Such spots would create flat-bottomed photospheric lines when highly rotationally broadened causing small bumps when the broadened template is subtracted.

Before subtracting the convolved templates, the ER Vul spectra had to be rebinned to the same 1.9 km s<sup>-1</sup> per pixel as the BFs and templates. A cross-correlation was then performed with IRAF’s *fxcor* routine of each ER Vul spectrum with its corresponding template, using only the photospheric flux between the H and K absorption lines gives the best alignment of the spectra before subtraction. The average measurement error in the velocity shift was 4.5 km s<sup>-1</sup> (or 2.4 pixels).

Both the broadened template and the ER Vul spectrum were normalized by fitting a low-order polynomial to the regions outside the H and K cores before subtraction. The templates were subtracted from the corresponding ER Vul spectra to isolate the chromospheric contribution. The residuals for all K lines are plotted in Figure 7 starting with  $\phi = 0.09$  at the bottom and individually plotted in Figures 8, 9 and 10.

## 4.2. Origins of Emission

For phases outside of conjunction, the residual K emission is well fitted with three Gaussian profiles indicating three separate origins. An example is shown in Figure 11. This is a necessary step to isolate the contributions made by each. The two narrower peaks are clearly the Ca II K emission from each of the stars. Neither the primary nor secondary star’s K emission strength appears to vary much throughout the orbit. Through their UV and X-ray observations, Vilhu & Rucinski (1983) suggest that there is a level at which the emission from RS CVn systems becomes saturated. Gunn & Doyle (1997) base their assumption that ER Vul’s chromospheric emission is close to saturation on the very large filling factor they

obtained. Saturation of the chromospheric emission may be another explanation for the lack of variation seen the K emission of the two stars. The extremely strong emission in practically every spectral activity indicator supports this possibility.

The third source is the is highly-redshifted broad emission between  $\phi = 0.09$  and  $0.39$ . It is shifted  $320 \text{ km s}^{-1}$  relative to the center velocity of K line. In Figure 12 (top), the Gaussian fits for the two stars were removed and the remaining broad emission for each phase in the range is overplotted. The average FWHM of the Gaussian fits to these is  $290 \text{ km s}^{-1}$ . The peaks do not shift much through this phase range either. During the opposite orbital phases,  $\phi = 0.60 - 0.90$ , the excess emission appears narrower with a FWHM ranging between  $130$  and  $270 \text{ km s}^{-1}$  and with smaller peaks. However, the peaks are again shifted  $320 \text{ km s}^{-1}$  from center but now blueward. The broad emission at each phase within this range is plotted in Figure 12 (bottom).

The scenario that best fits the observed Ca II emission from the ER Vul system includes: 1) high-latitude active regions on one or both of the stars that are covering large areas on the stellar surface and 2) a high-velocity stream of hot gas flowing on to the secondary in a widening spiral arriving on the surface at approximately  $30 - 60^\circ$  beyond the sub-binary longitude. The decreased flux of the stream during  $\phi = 0.60 - 0.90$  is due to its partial eclipse by the secondary. The change in velocity and flux of the broad emission is evident in Figure 13 where a sample of K residuals are overplotted onto their ‘opposite phase’ residuals.

The active region on each star is most likely not confined to a narrow longitudinal range but may cover as much as 50% of the hemisphere. However, it appears as if the center of the broad emission (and any associated surface hot spot) leads the sub-binary point by  $\sim 30 - 40^\circ$ . Plotting the integrated residual K flux as a function of orbital phase (Figure 14), we see an increase in K emission that peaks near  $\phi = 0.38$  and has a width of about 90 degrees. In this case, the reflection effect as the cause of the heating as suggested by Piskunov (1996) is not supported since the hot spot emitting the excess Ca II is not centered on the sub-binary point.

Our results are consistent with Zeinali et al. (1995) who also saw evidence of a gaseous stream flowing between the two components in their photometric data of ER Vul, however opposite in direction. More recently, Harmanec et al. (2004) interpreted phase-locked structure in their analysis of photometric data spanning over 50 years as evidence of gas streams that are projected against the disk of the primary at phases after secondary eclipse. In addition to streams, Arévalo et al. (1988) explained photometric peculiarities in ER Vul as due to circumstellar matter. Hall & Ramsey (1994) surveyed ten RS CVn binary systems (not including ER Vul) on which they have shown that large regions of extended, prominence-like material are common features with moderate- to high-velocity flows ranging from several

tens of  $\text{km s}^{-1}$  to  $170 \text{ km s}^{-1}$ . It is clear that high-velocity streams, prominences, and circumstellar material are all part of ER Vul’s dynamic environment.

At the very end of our observations, we caught a rather strong flare at  $\phi = 0.965$  as shown in Figure 15. It contains  $\approx 13\%$  more power than the emission at the other phases near conjunction. We cannot say from which star the flare originated.

## 5. The Photometric Light Curve

There is likely to be a spot on the surface of the secondary associated with the impact of the high-velocity stream of hot plasma. This is consistent with observations of a more active secondary as compared to the primary by Gunn & Doyle (1997) and Çakirli et al. (2003). A photospheric spot, however, is not detected as a travelling feature in the K residuals or the BFs, nor as a distortion in the RVs measured from the BFs.

Harmanec et al. (2004) executed concurrent photometric observations of ER Vul in order to search for photospheric indicators of activity. To investigate if a hot spot on the cooler star is consistent with the light curve of ER Vul, a suite of model light curves were generated using a recent version of the code described by Wilson & Devinney (1971) and Wilson (1979, 1990, 1993). The models were compared with normal points generated from the V-band light curve recorded at the same epoch as the spectroscopic observations.

The geometrical parameters of ER Vul were set first by considering spot-free models. ER Vul has been the object of a number of photometric investigations (e.g. Harmanec et al. 2004; Olah et al. 1994; Hill et al. 1990), and so the solution computed by Harmanec et al. (2004) from combined UBVR<sub>I</sub> and radial velocity data was used as a starting point. The temperatures of the two stars were fixed at the values adopted by Hill et al. (1990).

The final adopted inclination and mean stellar radii, computed after making minor adjustments to match the depths and widths of the eclipses, are summarized in Table 2. The ratio of the stellar radii is intermediate between the values found by Hill et al. (1990), who found that the components have the same radii, and Harmanec et al. (2004), who use  $r_2/r_1 = 0.64$ .

Table 2. Light curve model parameters

Parameter	Value
$i$	$67.99^\circ$
$r_1$	$0.291^a$
$r_2$	$0.240$
spot long	$36^\circ$
spot rad	$54^\circ$
spot temp	$1.015T_{eff,2}^b$

<sup>a</sup>in units of orbital separation

<sup>b</sup>the effective temperature of the secondary star

Keeping the geometric parameters fixed, a second set of runs were made in which a hot spot was added to the secondary, with parameters chosen to reproduce the magnitude difference between the out of eclipse maxima in the light curve. Preliminary experiments indicated that the spot must be close to the orbital plane, and so the latitude of the spot was fixed in the orbital plane for all subsequent runs. The spot parameters that were investigated in greater detail are (1) the longitude of the spot centroid, (2) the spot radius, and (3) the temperature of the spot with respect to that of the surrounding photosphere. The results were then compared with the light curves to identify those models that are best able to reproduce the outside eclipse light variations; the introduction of spots were found to have only a minor impact on the eclipse minima.

The models that best match the data favor a spot on the hemisphere of the (cooler) secondary star facing the (hotter) primary star, but with a center that is offset by  $30 - 40^\circ$  from the line connecting the two stars - - in excellent agreement with the phase at which the peak Ca II emission is seen in Figure 14. In addition, large spots that cover an entire hemisphere of the cooler star’s surface and have temperatures that are 1 - 2% hotter than the undisturbed photosphere are better able to match the out of eclipse light variations than models with smaller spots and hotter temperatures.

The model that best matches the light curve is shown in Figure 16, and the spot parameters used in this simulation are listed in Table 2. The light curve generated without spots is also shown for comparison. The agreement between the model with spots and the observations shows systematic differences outside of eclipse, and it is conceivable that models that include refined physics, such as multiple spots, third light from a stream, and/or temperature structure within the spot(s) may give better agreement with the data.

## 6. Conclusions

We have presented 42 high-quality Ca II H & K spectra from the CFHT that cover nearly the entire 17-hour orbit of ER Vul in search of phase-dependent chromospheric activity. The rapid rotation causes severe line-blending and broadening such that it is difficult to distinguish between the spectra of the two stars. To do this, we invoked the Broadening Function Formalism. We calculated BFs from the photospheric absorption lines outside of the H and K lines, convolved a sharp-lined spectrum with the BF at each orbital phase, and then subtracted the convolved template from the corresponding ER Vul spectrum. The residuals consisted of only Ca II chromospheric emission. We focus only on the K line since the H line suffered from end effects.

The K emission appears to come from three different locations in the system: the primary star, the secondary star and a broad stream flowing towards the secondary at a velocity of  $320 \text{ km s}^{-1}$ . The in-falling material from the stream onto the secondary enhances the emission from that region indicated by a) an increase in total observed K emission and b) a hot spot on the photosphere as seen in a concurrent photometric lightcurve. Both are consistent with an active region leading the sub-binary longitude by  $30 - 40^\circ$ .

ER Vul is not an ideal amplified analog of planet-induced stellar activity. Few 51 Peg primaries have spun up into synchronous rotation, thereby energizing the dynamo level seen in ER Vul and the 51 Peg secondaries are likely to be tidally locked and therefore may have less extensive magnetic fields than Jupiter. None the less, it is interesting to note that the chromospheric activity of HD179949 was synchronized with the 3.1 d revolution period of the secondary for two years (Shkolnik et al. 2003, 2004) with the active region on the primary preceding the sub-planetary point by some 0.2 in phase, similar to the leading spot on ER Vul's secondary.

Research funding from the Canadian Natural Sciences and Engineering Research Council (G.A.H.W., S.R., & E.S.) and the National Research Council of Canada (D.A.B., T.D.) is gratefully acknowledged. We are also indebted to the CFHT staff for their care in setting up the CAFE fiber system and the Gecko spectrograph. We would also like to thank Petr Harmanec, Russ Robb, and the paper's referee for useful discussion and commentary.

## REFERENCES

- Arévalo, M.J., Lazaro, C., Fuensalida, J.J., 1988, *AJ*, 96, 1061.
- Baudrand, J., Vitry, R., 2000, *Proceedings of the SPIE*, 4008, 182.
- Çakirli, O., Ibanoglu, C., Frasca, A., Catalano, S., 2003, *A&A*, 400, 257.
- Catalano, S., Rodanò, M., Frasca, A., Cutispoto, P., 1996, *Stellar Surface Structure*, IAU Symp. 176, 403.
- Collier Cameron, A., Horne, K., Penny, A., James, D., 1999, *Nature*, 402, 751.
- Collier Cameron, A., Donati, J.-F., Semel, M., 2002, *MNRAS*, 330, 699.
- Donati, J.-F., Henry, G.W., Hall, D.S., 1995, *A&A*, 293, 107.
- Donati, J.-F., Semel, M., Carter, B.D., Rees, D.E., Collier Cameron, A., 1997, *MNRAS*, 291, 658.

- Duemmler, R., Doucet, C., Formanek, F., Ilyin, I., Tuominen, I., 2003, *A&A*, 402, 745.
- Fernandez-Figueroa, M.J., Montes, D., De Castro, E., Cornide, M., 1994, *ApJS*, 90, 433.
- Glebocki, R., Bielicz, E., Pastuszka, Z., Sikorski, J., 1986, *AcA*, 36, 369.
- Groot, P.J., Piters, A.J.M., van Paradijs, J., 1996, *A&AS*, 118, 545.
- Guedel, M., Guinan, E.F., Skinner, S.L., 1997, *ApJ*, 483, 947.
- Gunn, A.G., Doyle, J.G., 1997, *A&A*, 318, 60.
- Hall, D.S., 1992, *ASPC*, 34, 27.
- Harmanec, P., Božić, H., Robb, R.M., Ruždjak, D., Sudar, D., Thanjavur, K., 2004, *A&A*, 415, 289.
- Lanza, A.F., Rodonò, M., Mazzola, L., Messina, S., 2001, *A&A*, 376, 1011.
- Linsky, J.L., 1980, *ARA&A*, 18, 439.
- Mariska, J.T., 1992, *The Solar Transition Region*, Cambridge University Press.
- Messina, S., Rodonò, M., Guinan, E.F., 2001, *A&A*, 366, 215.
- Messina, S., Guinan, E.F., 2002, *A&A*, 393, 225.
- Montes, D., Fernandez-Figueroa, M.J., de Castro, E., Cornide, M., 1994, *A&A*, 285, 609.
- Montes, D., Fernandez-Figueroa, M.J., Cornide, M., de Castro, E., 1996, *A&A*, 312, 221.
- Olah, K., Budding, E., Kim, H-I, Etzel, P.B., 1994, *A&A*, 291, 110.
- Pasquini, L., de Medeiros, J.R., Girardi, L., 2000, *A&A*, 361, 1011.
- Piskunov, N.E., 1996, *Stellar Surface Structure*, IAU Symp. 176, 45.
- Reiners, A., Schmitt, J.H.M.M., 2003, *A&A*, 412, 813.
- Rubenstein, E.P., Schaeffer, B.E., 2000, *ApJ*, 529, 1031.
- Rucinski, S.M., 1992, *PASP*, 104, 1177.
- Rucinski, S.M., 1998, *PASP*, 110, 272.
- Rucinski, S.M., 1999, *Precise Stellar Radial Velocities*, eds. J.B. Hearnshaw & C.D. Scarfe, ASP Conf. Vol.185, p.82.



- Rucinski, S.M., 2002, *AJ*, 124, 1746.
- Shkolnik, E., Walker, G.A.H., Bohlender, D.A., 2003, *ApJ*, 597, 1092.
- Shkolnik, E., Walker, G.A.H., Bohlender, D.A., Gu, P.-G., Kürster, M., 2004, *ApJ*, 655, 1075.
- Sokoloff, D., Piskunov, N., 2002, *MNRAS*, 334, 925.
- Vogt, S.S., Hatzes, A.P., Misch, A.A., Kürster, M., 1999, *ApJS*, 121, 547.
- Walker, E.C., 1944, *JRASC*, 38, 249.
- Walker, G.A.H., Shkolnik, E., Bohlender, D.A., Yang, S., 2003, *PASP*, 115, 700.
- White, N.E., Parmar, A.N., Sweeney, M.A., Culhane, J.L., 1987, *MNRAS*, 227, 545.
- Wiedemann, G., Deming, D., Bjoraker, G., 2001, *ApJ*, 546, 1068.
- Wilson, R.E., 1979, *ApJ*, 234, 1054.
- Wilson, R.E., 1990, *ApJ*, 356, 613.
- Wilson, R.E., 1993, in *New Frontiers in Binary Star Research*, ed. K-C Leung & I-S Nha (ASP: San Francisco), p. 91.
- Wilson, R.E., Devinney, E.J., 1971, *ApJ*, 166, 605.
- Zeinali, F., Edalati, M.T., Mirtorabi, M.T., 1995, *IBVS*, 4190, 1.

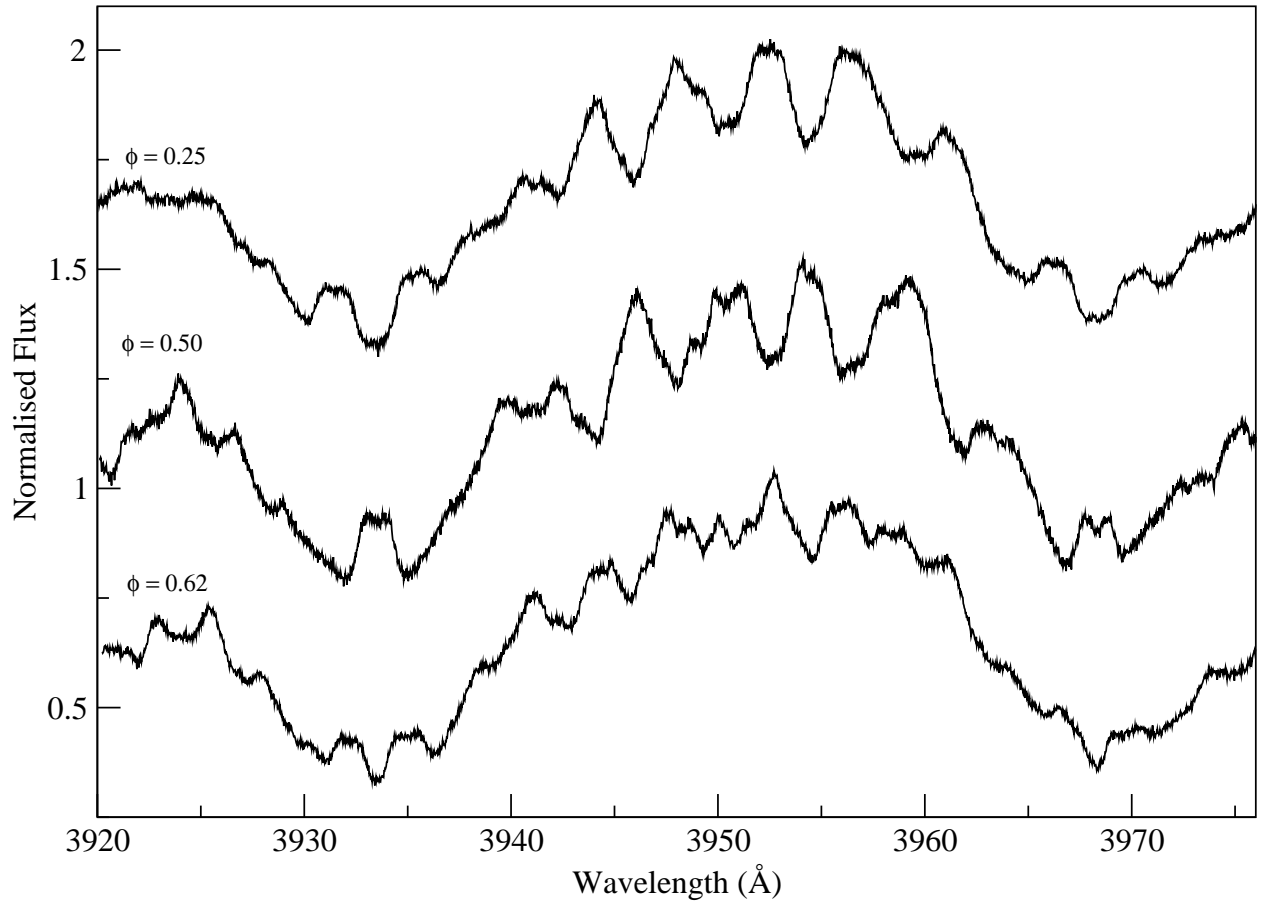


Fig. 1.— ER Vul spectra normalized to the peak intensity at three orbital phases.

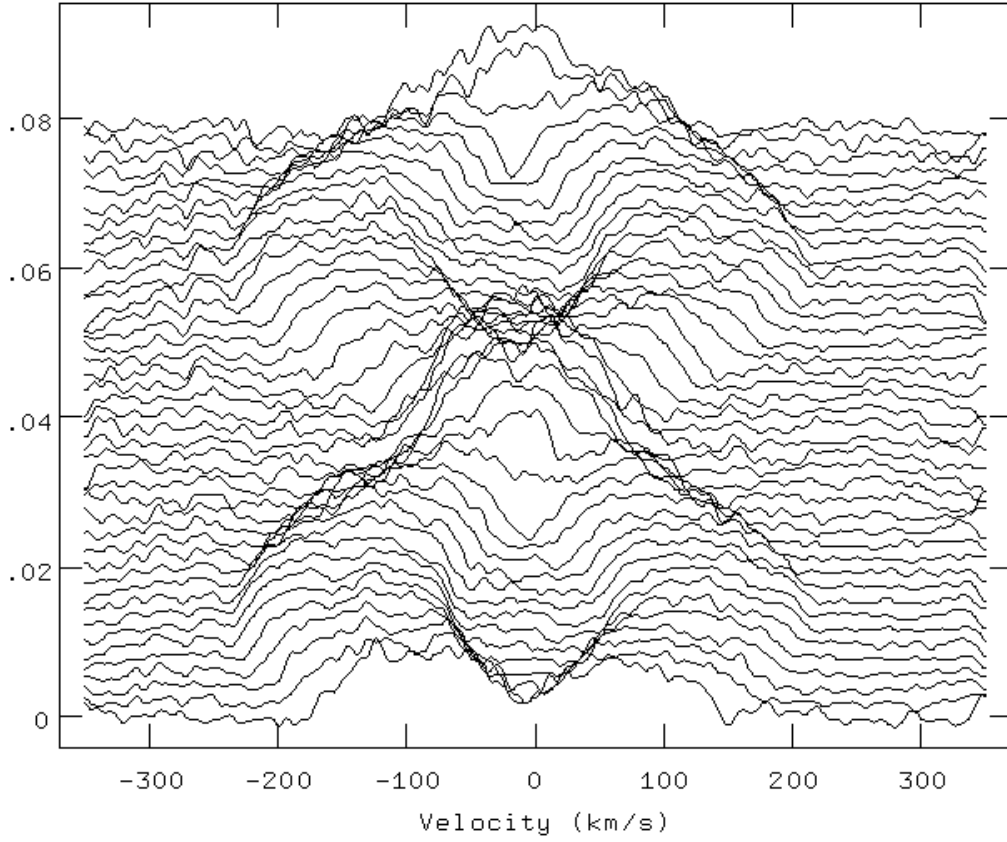


Fig. 2.— The broadening functions of ER Vul for all data starting with  $\phi = 0.09$  (bottom curve) to 0.96 (top curve) as a function of BF intensity. The intensities are normalized but are displaced vertically.

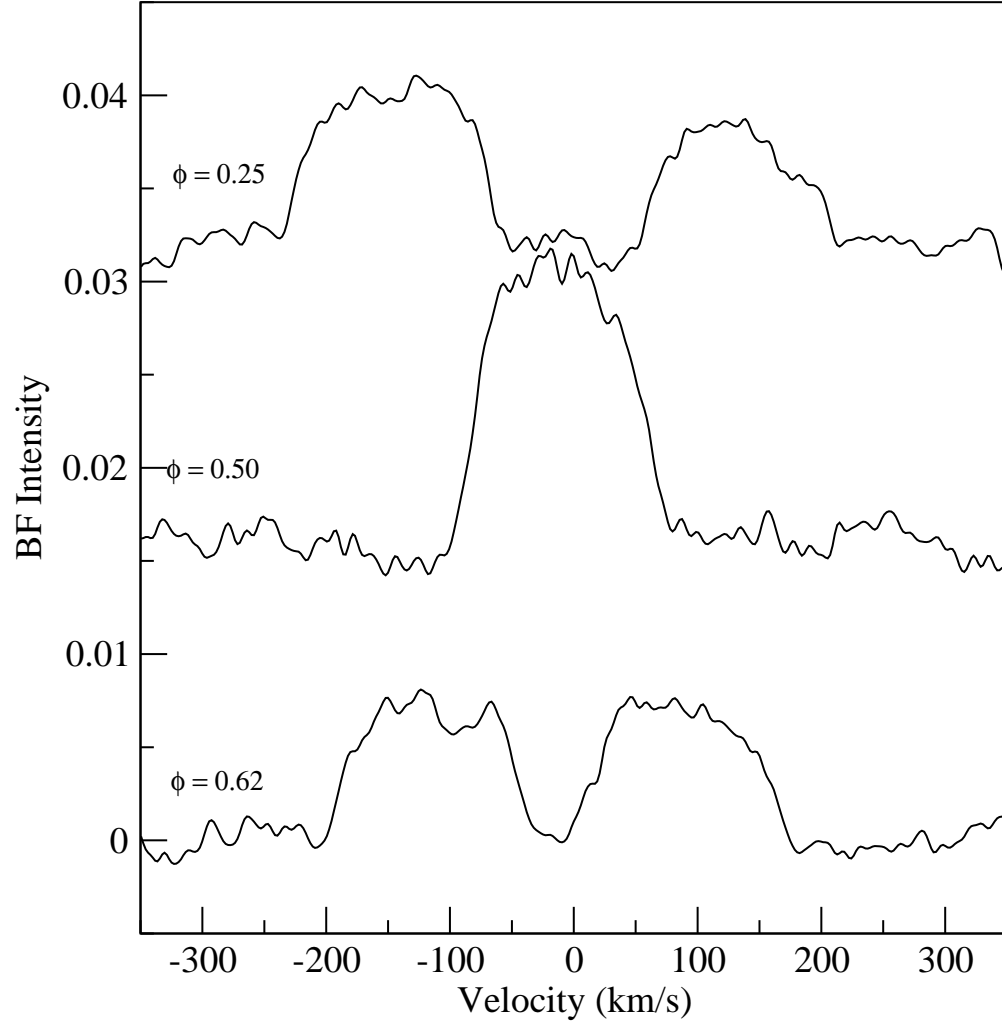


Fig. 3.— Examples of broadening functions at three orbital phases.

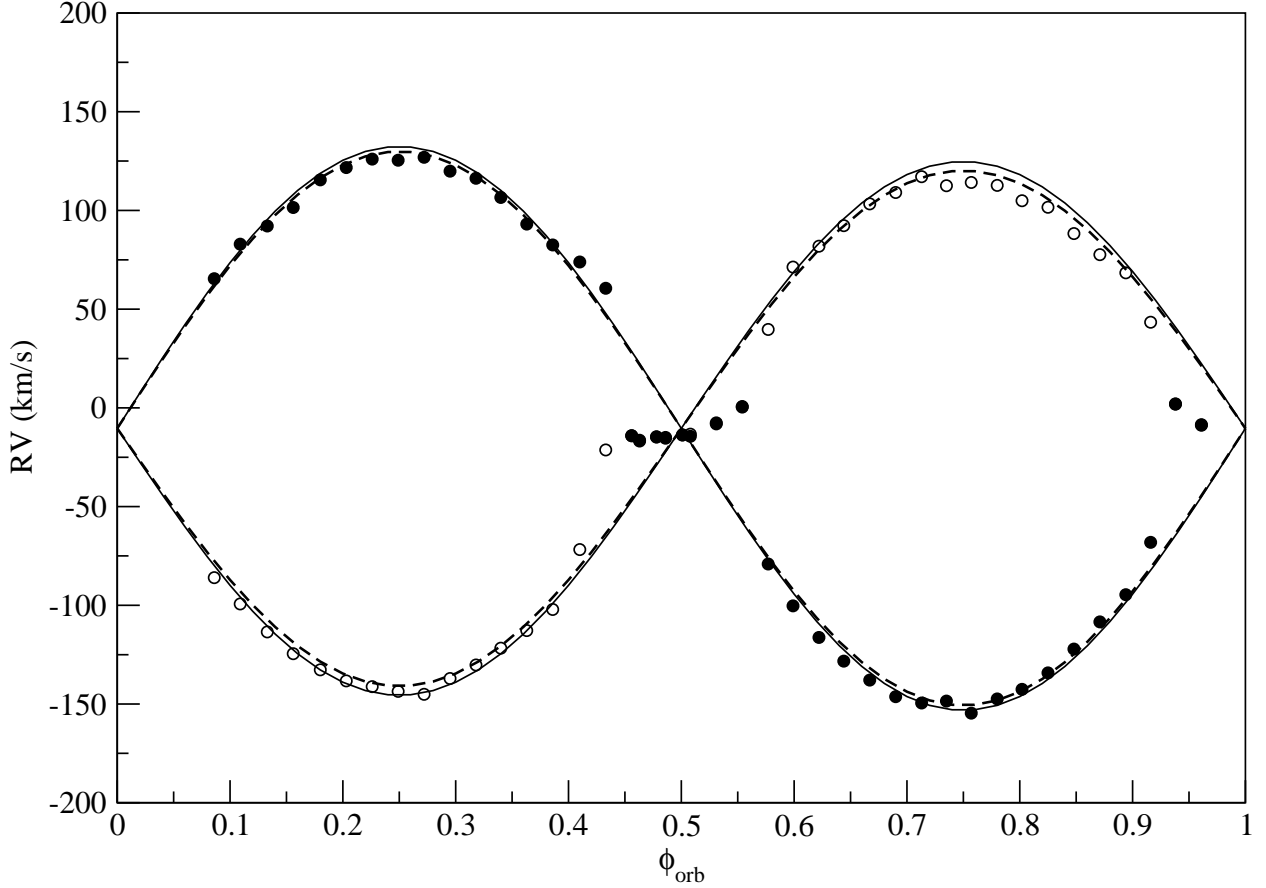


Fig. 4.— The ER Vul radial velocities determined from the BFs as a function of orbital phase. The RVs of the primary are represented by the open circles, and the secondary by the filled circles. The data are listed in Table 1. The solid curves are orbital fits using values from Duemmler et al. (2003) and the dashed curves are the least-squares best fits to our data. See text for more details. The uncertainties in the RVs is  $\approx 0.5 \text{ km s}^{-1}$  for the values outside of the eclipses. During the eclipses, the BFs of the components are blended making the RVs difficult to measure. The error in  $\phi$  is  $< 0.0001$  since the ephemeris is very well known.

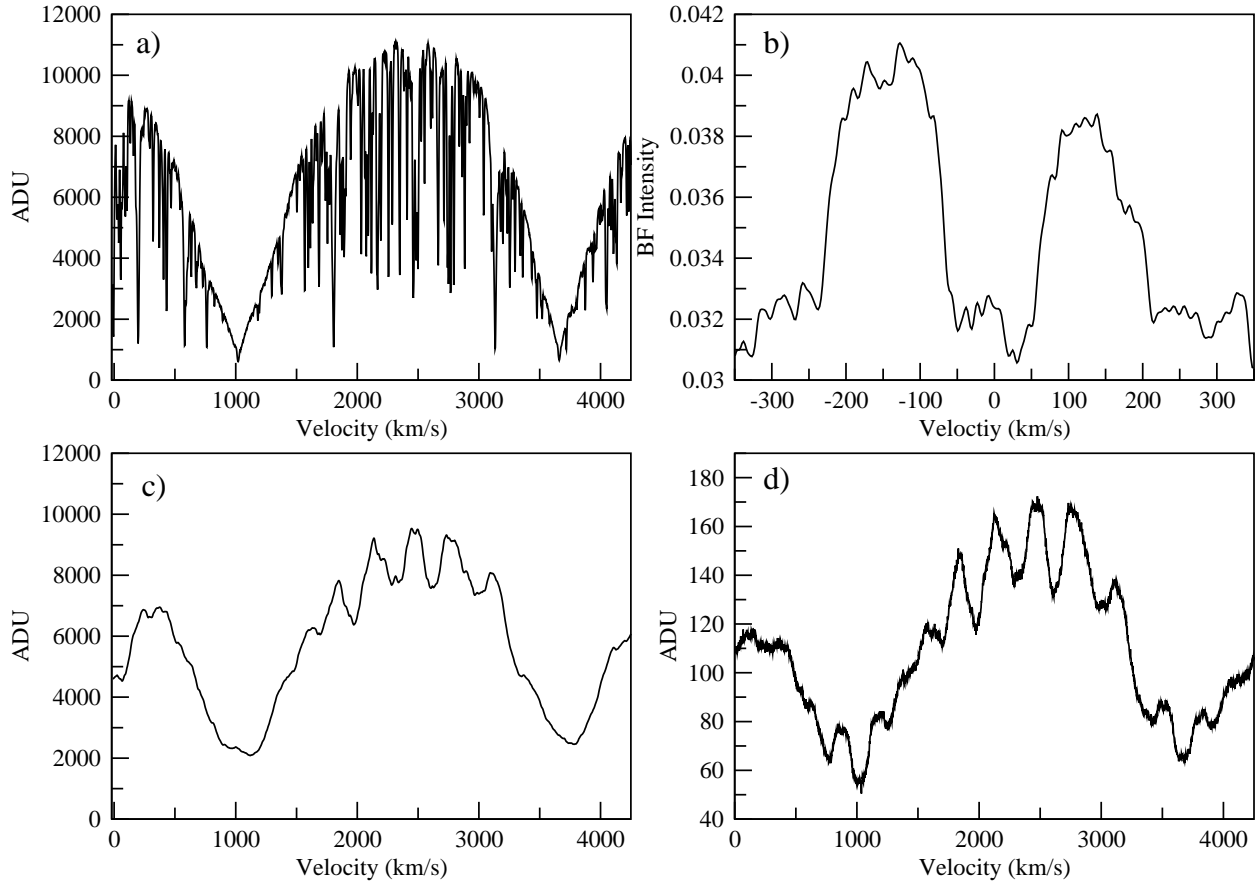


Fig. 5.— a) The template spectrum of the sharp-lined star HD 209458. b) The BF calculated for  $\phi = 0.25$ . c) The convolution of the template spectrum with the BF. d) The ER Vul spectrum at  $\phi = 0.25$ .

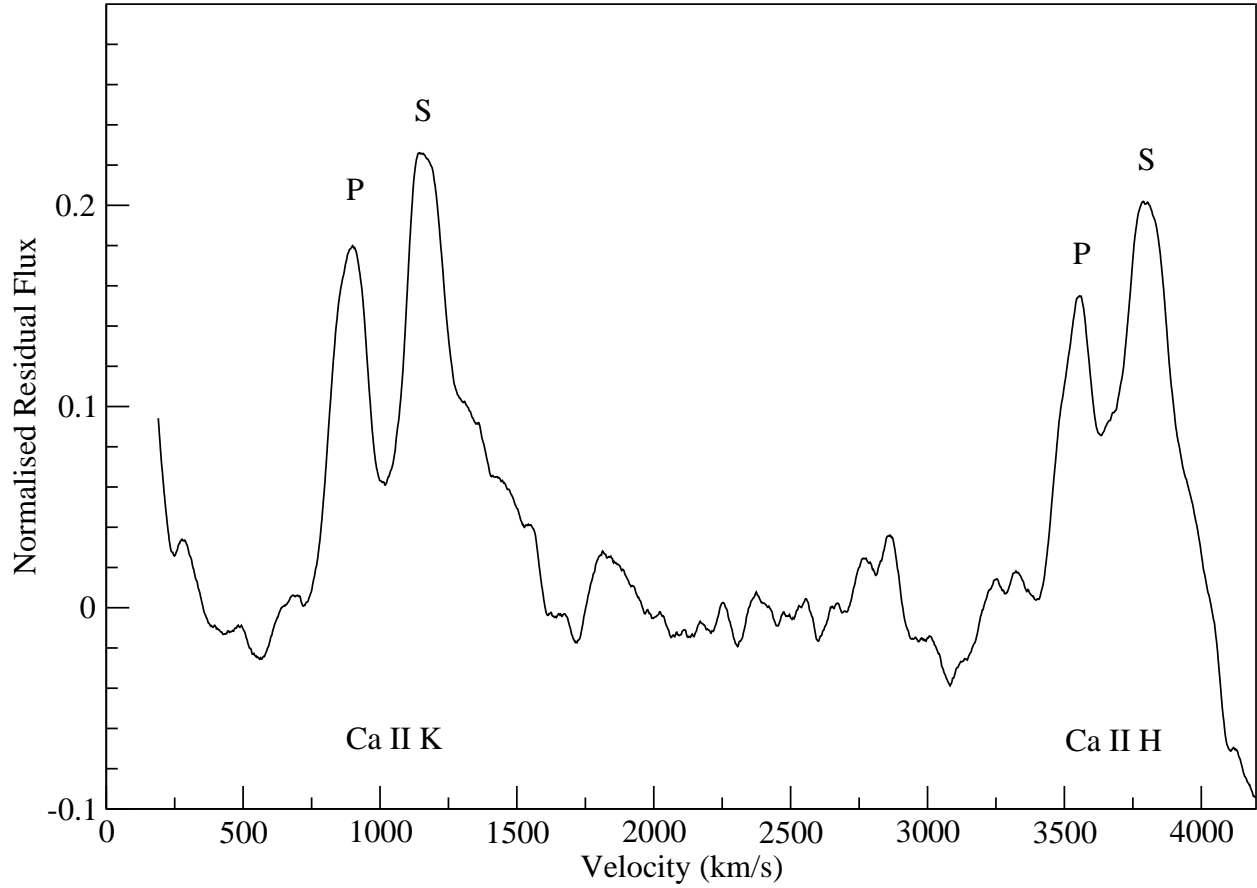


Fig. 6.— The full Ca II H & K residual spectrum of the broadened template subtracted from the corresponding ER Vul spectrum at  $\phi = 0.25$ . The emission from the primary and secondary are labeled ‘P’ and ‘S’, respectively.

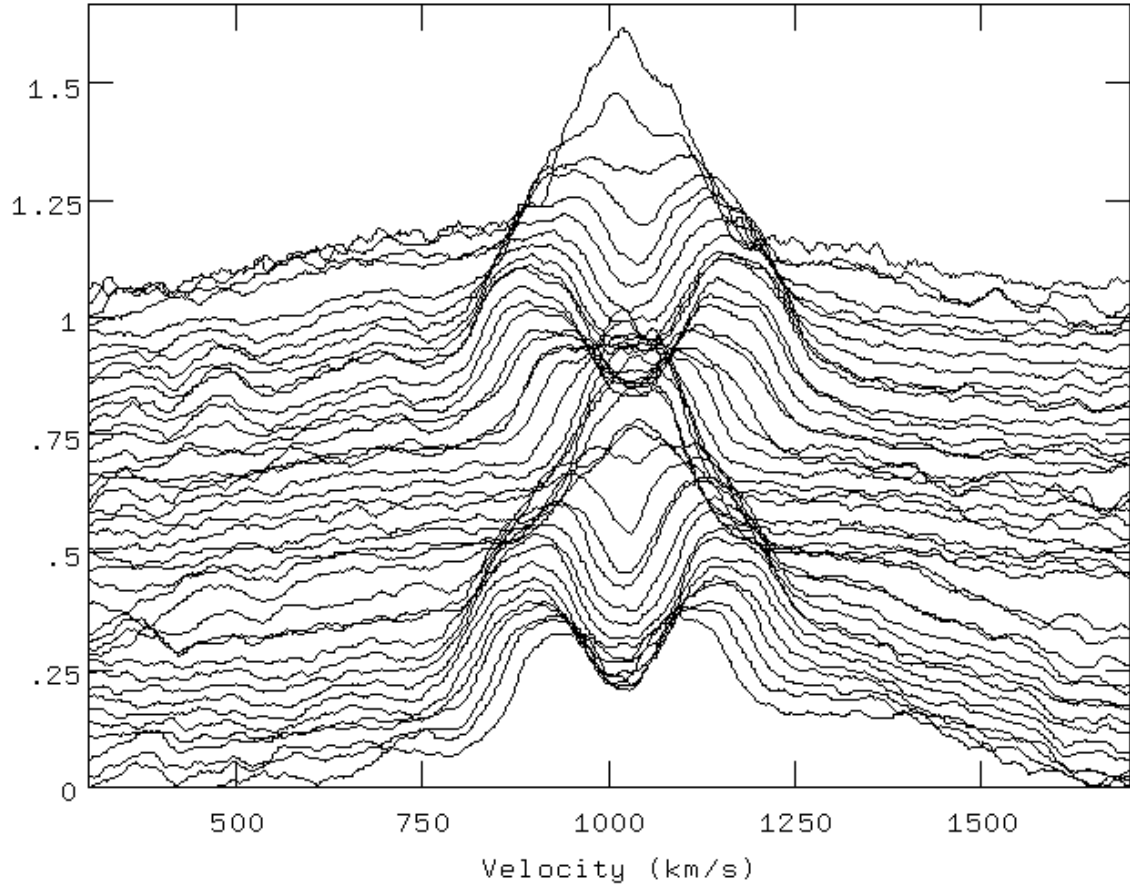


Fig. 7.— The Ca II K emission of ER Vul (smoothed by 9 pixels) at all observed phases starting at  $\phi = 0.09$  (bottom curve) to 0.96 (top curve). The vertical axis is normalized residual flux with arbitrary vertical shift.



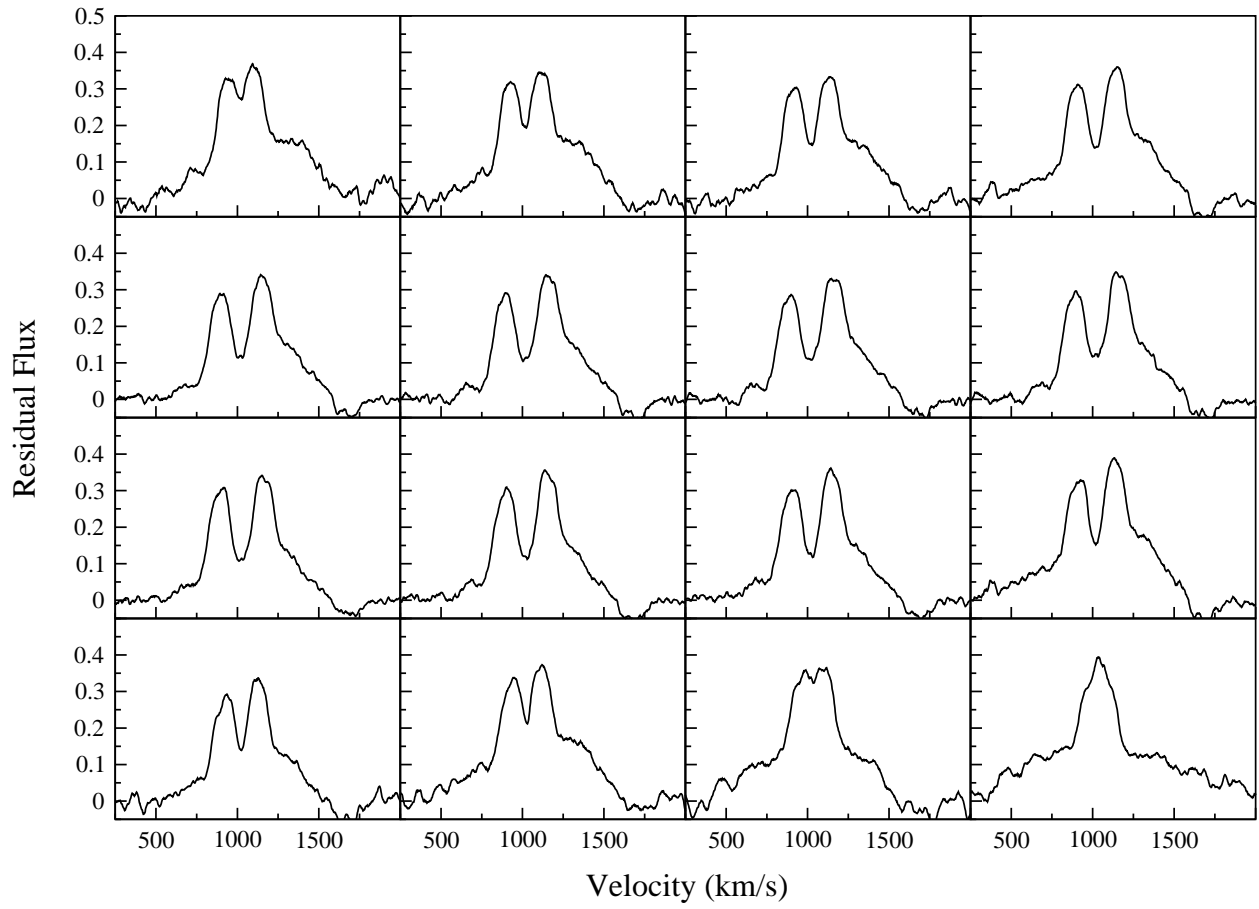


Fig. 8.— Ca II K residual emission for phases ranging from 0.090 to 0.437.

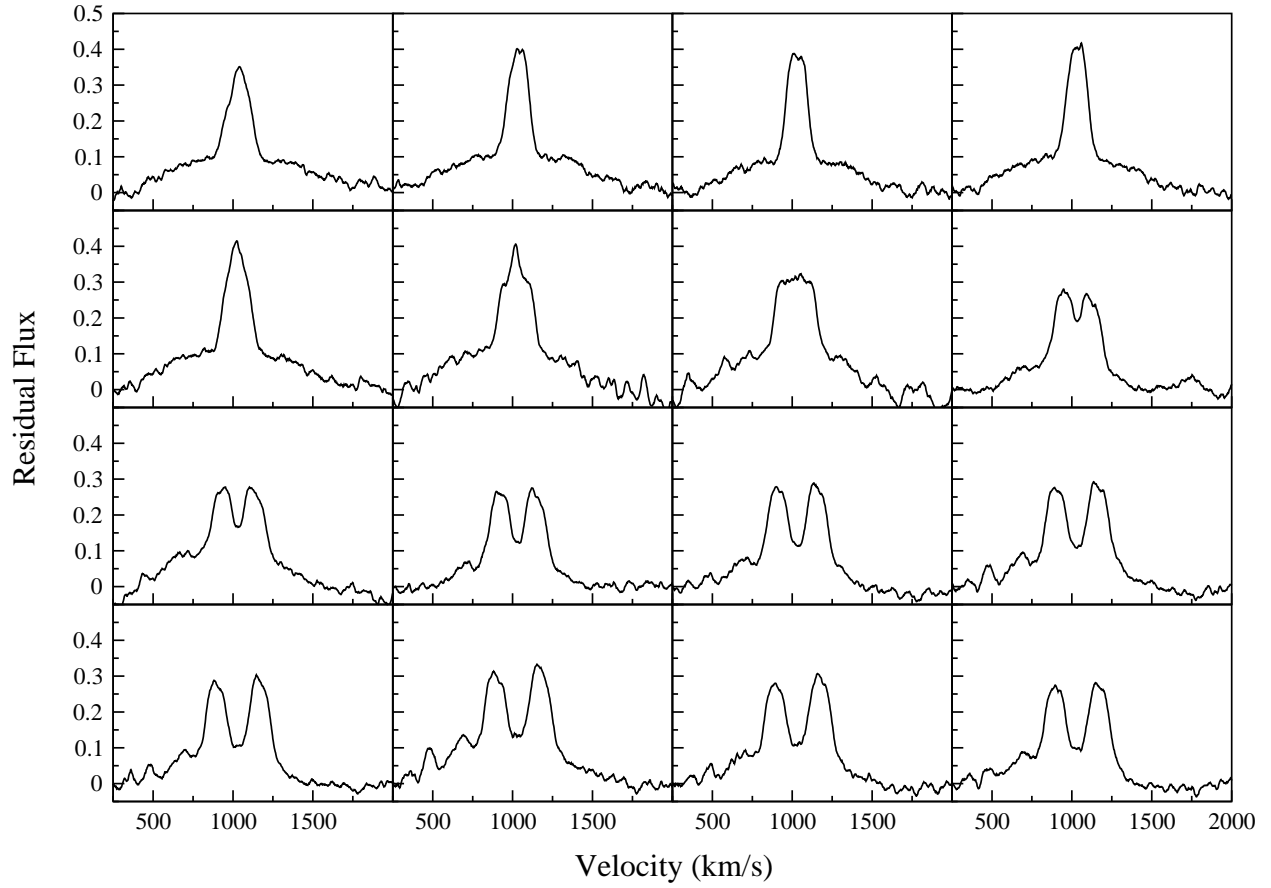


Fig. 9.— Ca II K residual emission for phases ranging from 0.460 to 0.761.

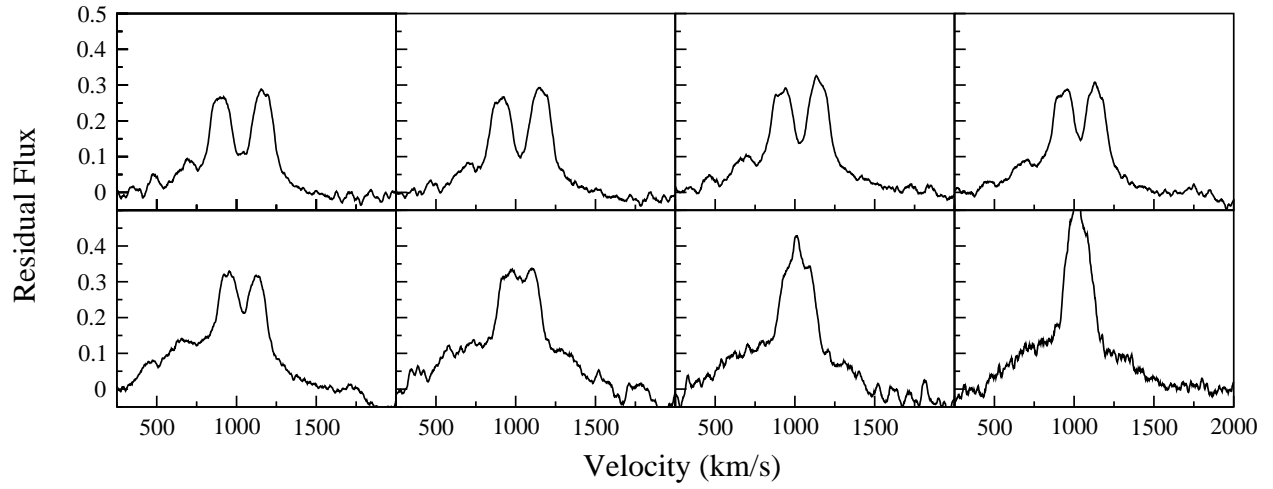


Fig. 10.— Ca II K residual emission for phases ranging from 0.781 to 0.965.

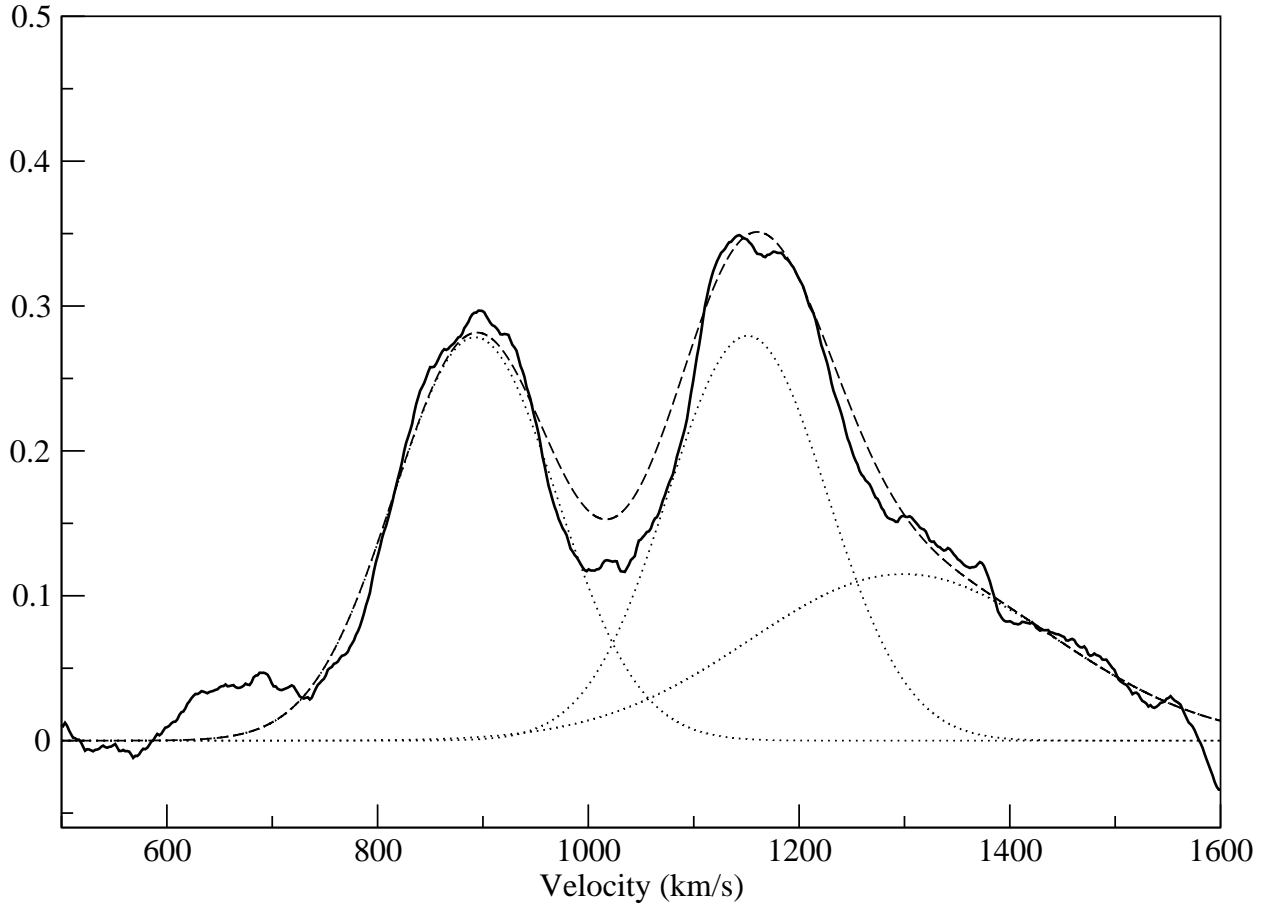


Fig. 11.— The K emission for  $\phi = 0.25$  (solid curve) deblended into three Gaussians (dotted curves). The dashed curve is the sum of the three Gaussians.

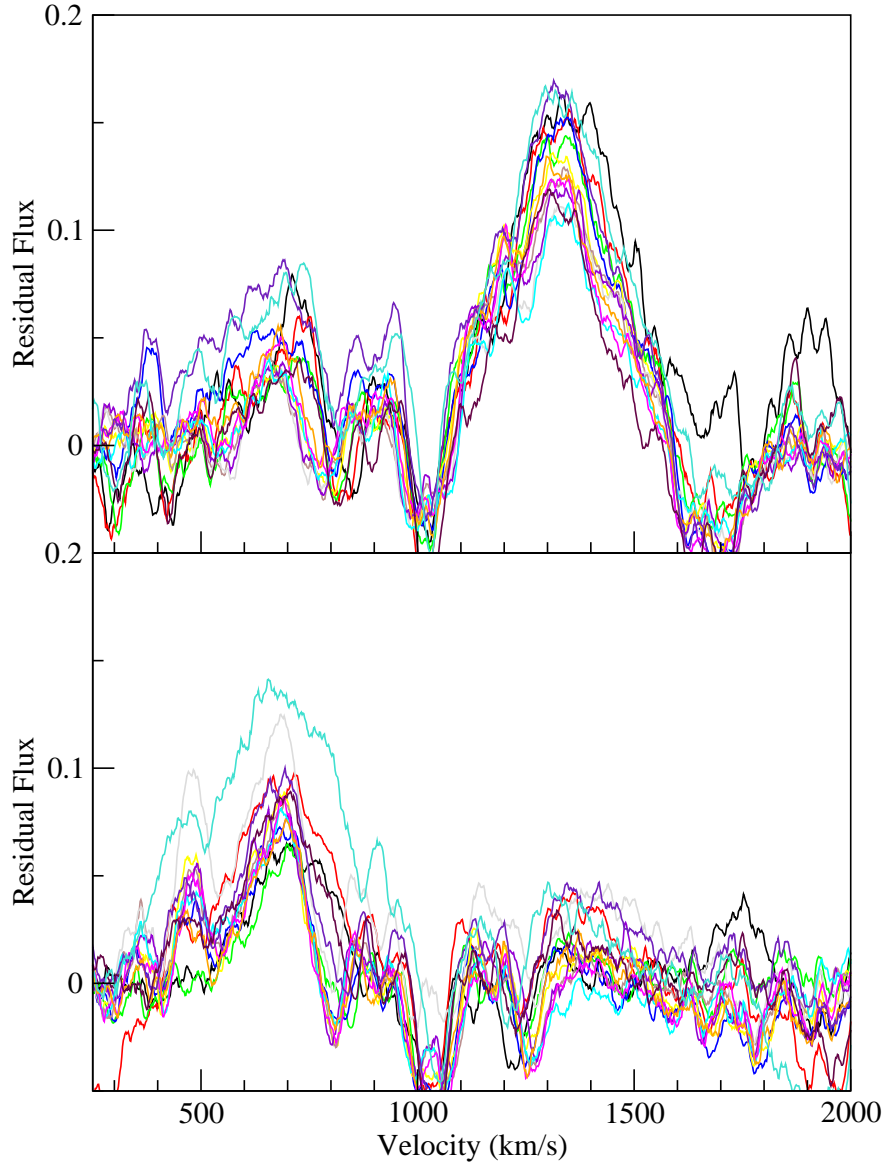


Fig. 12.— The broad emission after the K emission from the two stars has been subtracted overlaid (excluding phases nearing conjunction); Top: from  $\phi = 0.090 - 0.39$  and Bottom:  $\phi = 0.603 - 0.898$

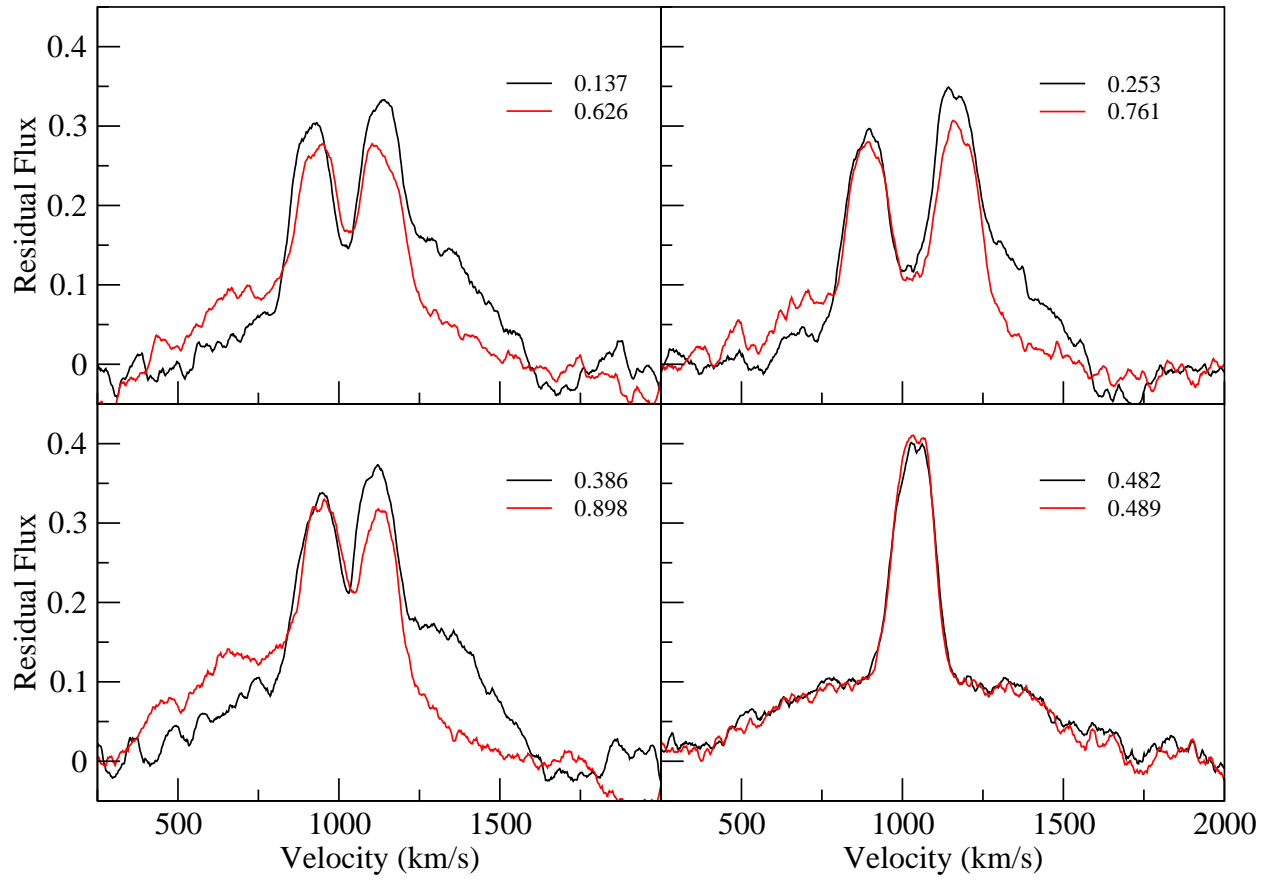


Fig. 13.— Ca II K residuals at opposite phases, except for the last panel that shows residuals at nearly the same phase but taken on two different nights.

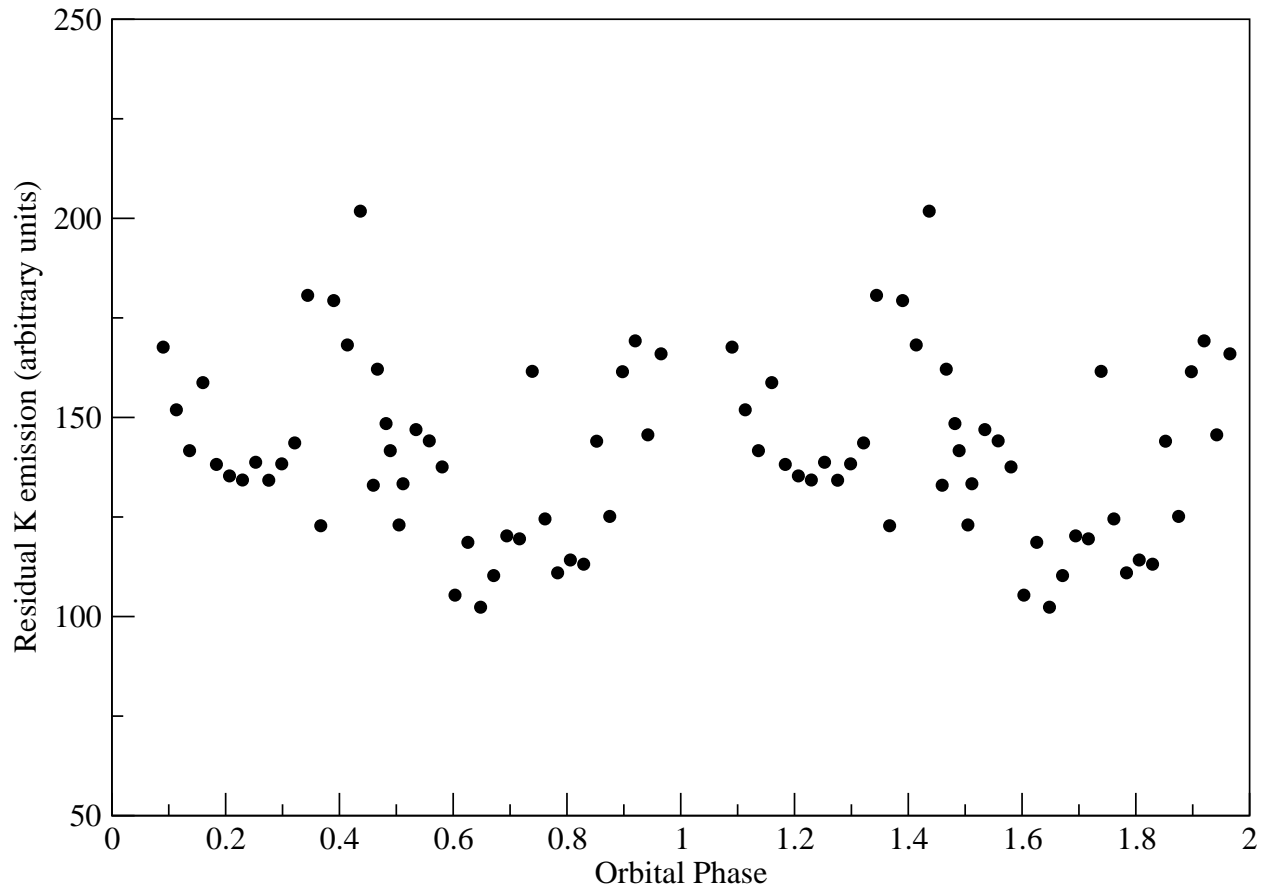


Fig. 14.— The integrated Ca II K emission of the residuals displayed in Figures 8, 9, 10.

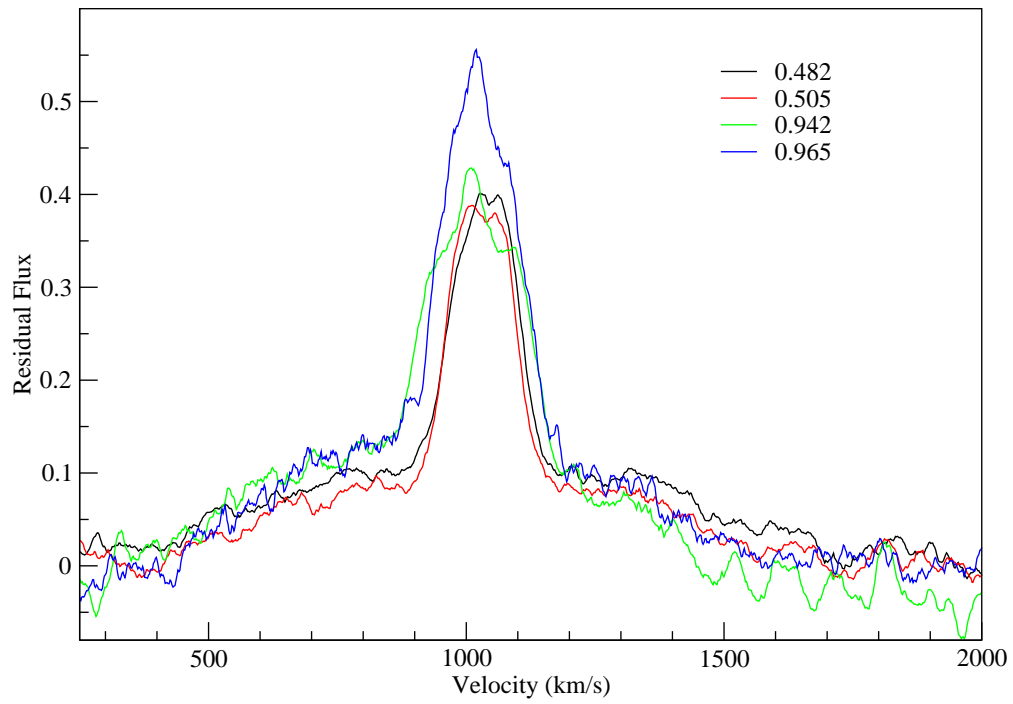


Fig. 15.— Ca II K residual emission during four phases near conjunction. Note the effect of a flare at  $\phi = 0.965$ .



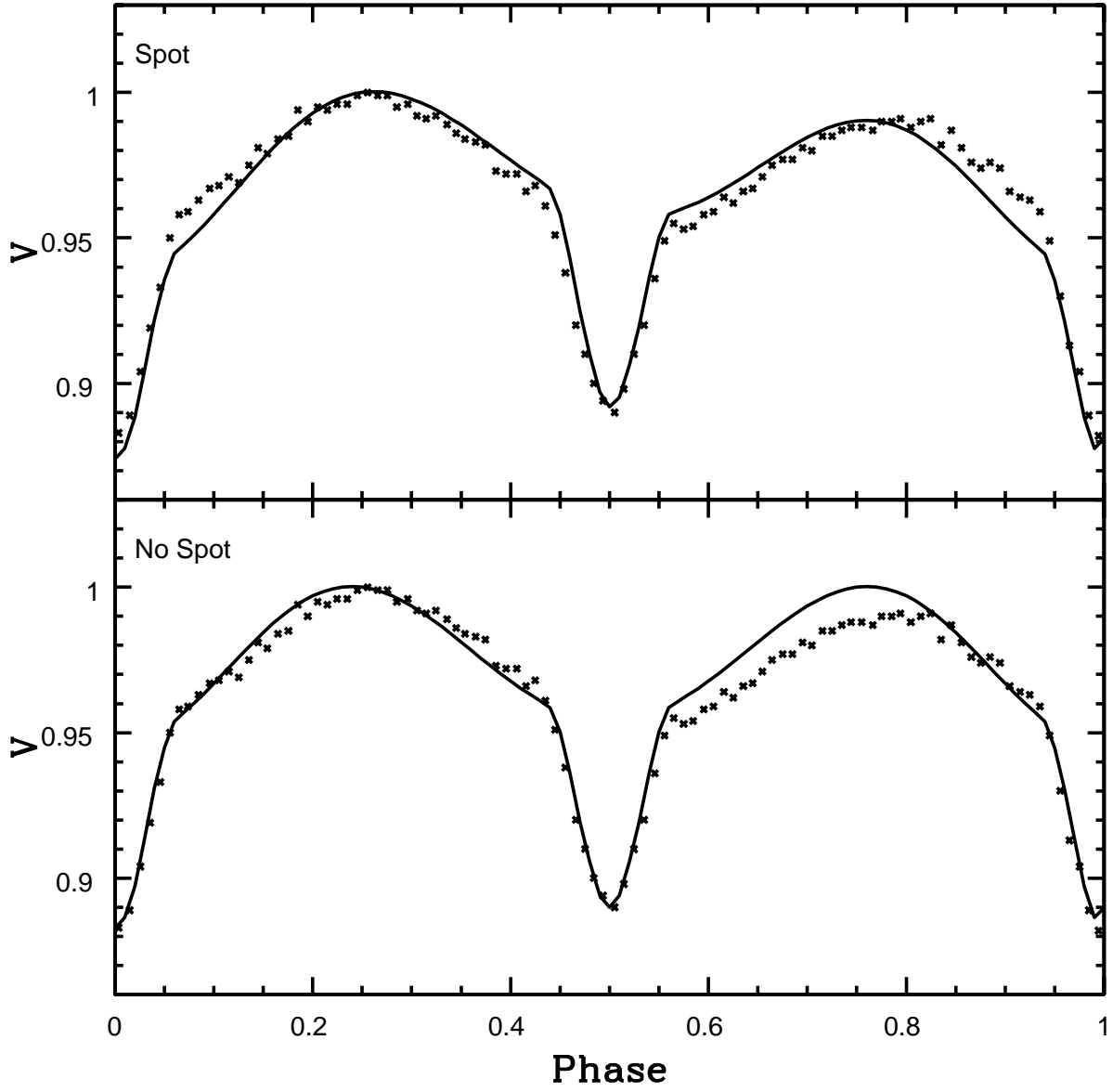


Fig. 16.— V-band normal points compared with model light curves with (top panel) and without (lower panel) a hot spot on the cooler star.